Eur. J. Mineral., 34, 539–547, 2022
https://doi.org/10.5194/ejm-34-539-2022

European Journal of Mineralogy
Open Access

Corresponding relationship between characteristic birefringence, strain, and impurities in Zimbabwean mixed-habit diamonds revealed by mapping techniques

Chengyang Sun[1,2], Taijin Lu[2], Mingyue He[1], Zhonghua Song[2], and Yi Deng[1]

[1]School of Gemology, China University of Geosciences, Beijing, 10083, China
[2]National Gems & Jewelry Testing Co. Ltd., Beijing, 100013, China

Correspondence: Taijin Lu (taijinlu@hotmail.com) and Mingyue He (hemy@cugb.edu.cn)

Received: 19 July 2022 – Revised: 11 September 2022 – Accepted: 22 October 2022 – Published: 9 November 2022

Abstract. Birefringence in diamond is an optical phenomenon related to strain and various defects in crystal lattices. Despite extensive investigations being done to characterize and quantify it, there is still controversy about its origin in diamond lattices. Here we report the relationship between the distribution of birefringence patterns observed under cross-polarized light, strain features analyzed by Raman mapping, and the impurity characteristics revealed by Fourier transform infrared spectroscopy (FTIR) mapping in natural mixed-habit diamonds. It was deduced that the plastic deformation was enhanced with higher tensile residual stress, and nitrogen and VN_3H defects were more enriched as a result of the temperature increase during crystallization, at growth bands showing straight birefringence patterns and the relative enrichment of graphite inclusions. These results provided solid data and insights for birefringence-related properties in diamond and correlated the occurrence of birefringence with diamond spectroscopic properties, which promoted the understanding of the formation of birefringence in natural diamonds and would be helpful for the synthesis of high-quality, birefringence-free diamonds.

1 Introduction

Diamond is an important mineral that forms in the mantle (Bureau et al., 2016), whose characteristics, such as morphology, inclusions, defects, strain, birefringence, and isotopic characteristics, could reveal massive detailed information about the geochemical environment in which it crystallized (Skuzovatov et al., 2011) as well as the migration process of C–H–O fluids in the mantle and the tectonic movement it had experienced before being ejected to the Earth's surface (Zedgenizov et al., 2004; Weiss et al., 2009). Therefore, it is crucial to examine characteristics of diamonds and look into their causes, especially for naturally occurring diamonds with distinctive features that may reveal important new information about geological processes taking place deep inside the Earth.

Based on the theory of crystal optics, diamond, the typical isotropic mineral, should exhibit total extinction under cross-polarized light. However, natural diamonds almost always show birefringence due to defects like cracks, dislocations, inclusions, plastic deformation, and lattice parameter variations (Lang, 1967; Agrosì et al., 2013). To quantitatively analyze this optical phenomenon of photo-elastic effect caused by strain (Howell, 2012), considerable experimental work has been performed to quantify the photo-elastic constants of diamond (Grimsditch et al., 1979) as well as the relationship between its refractive index and the ambient pressure (Balzaretti and Dajornada, 1996). Also, extensive investigations have been undertaken to quantify strain, residual stress, and birefringence in diamonds (Kurtz et al., 1956; Glazer et al., 1996; Nasdala et al., 2005; Howell et al., 2010). Currently, the strength of birefringence has been widely used to evaluate the crystalline quality of synthetic diamonds (Masuya et al., 2017), and researchers have been actively looking for methods to eliminate defects and birefringence in diamond to produce perfect crystals (Chen et al., 2020). In addition to the birefringence caused by inclusions, dislocations, cracks, etc., natural mixed-habit diamonds (referring to nat-

ural diamond crystals showing both octahedral {111} facets and hummocky cuboid {100} surfaces) are characterized for two other types of birefringence patterns: one is the birefringence that shows straight patterns consistent with the shape of the growth band in the long range, which was thought to be generated by lattice parameter variation between different growth sectors (Sellschop, 1992), and the other is the birefringence caused by dense directional micro-cracks in cuboid sectors – around every micro-crack under cross-polarized light, there were black lobes that passed across the entire plane and revolved around the major axis of each oval micro-crack (Sun et al., 2022).

Spectroscopic characteristics of natural mixed-habit diamond had been studied to reveal the differential distribution of defects in different growth sectors (Lang et al., 2007; Howell et al., 2012a), and these characteristics have been compared to those of HPHT synthetic diamonds (Boyd et al., 1988; Burns et al., 1990; Smith and Wang, 2016), in which the impurities are more controllable. Impurity characteristics of natural mixed-habit diamonds can be summarized as follows: nitrogen-related absorption is stronger in octahedral sectors, which correlates with higher nitrogen concentrations, but the aggregation rates of nitrogen in different growth sectors seem to be at the same level (Howell et al., 2012b). Hydrogen-related absorption peaks are stronger in cuboid sectors, while the absorption intensity does not directly reflect the concentration of hydrogen. Because not all hydrogen in diamond exists in IR-active forms (Connell et al., 1998), irradiation-related defects also appeared in Zimbabwean mixed-habit diamonds due to the long residency in conglomerate containing radioactive minerals (Nasdala et al., 2013; Smit et al., 2018), and all these defects may transform differently in octahedral and cuboid sectors during the annealing process (Eaton-Magaña et al., 2017). In addition, in contrast to HPHT synthetic diamonds in which nickel atoms mainly concentrate in octahedral sectors (Kanda and Watanabe, 1997), nickel-related centers in natural mixed-habit diamonds are stronger in cuboid sectors (Lang et al., 2004; Howell et al., 2013).

The occurrence of birefringence in diamond may reveal the existence of defects and reflect the geological history of the diamond. However, to the best of our knowledge, few studies had explicitly illustrated the relationship between birefringence and spectroscopic properties of diamond. Based on the fact that birefringence, strain, and absorption peaks could all be related with impurities in diamonds, and mapping techniques could intuitively disclose spectroscopic characteristics of the full sample without compromising accuracy (Agrosì et al., 2017), in this study we took Zimbabwean mixed-habit diamonds for an example and used a polarized microscope to observe the distribution of inclusions and birefringence patterns, Raman mapping to analyze the degree of plastic deformation and the strength of residual stress, and micro-FTIR (Fourier transform infrared spectroscopy) mapping to reveal the differential distribution of impurities in different growth sectors. It was found that the growth bands showing straight birefringence patterns in octahedral sectors and the growth bands enriched with graphite inclusions in cuboid sectors presented similar anomaly characteristics in both Raman maps and FTIR maps, which provided new insights for us to understand the optical and spectroscopic properties of natural diamonds.

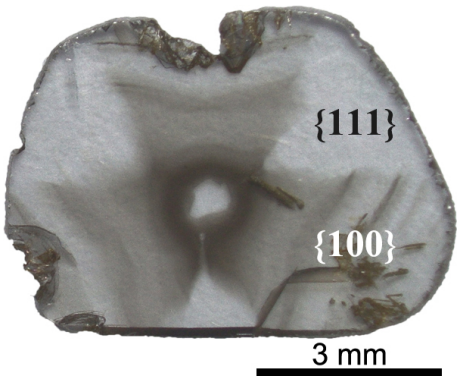

Figure 1. The Zimbabwean mixed-habit diamond section, NDS-2, cut off along {111} planes of the diamond crystal. The brown regions with dense inclusions are cuboid growth sectors, and the inclusion-free colorless regions are octahedral growth sectors.

2 Materials and methods

This study was based on 10 Zimbabwean mixed-habit diamonds collected from Marange deposits. These samples were cut parallel to {111} planes and polished into triangular sections. Five sections with the most prominent characteristic of mixed-habit were selected, which all displayed the correlations. One section labeled as "NDS-2" was taken as an example to demonstrate this finding (Fig. 1). This section is about 7 mm long, 5 mm wide, and less than 1 mm thick. These heavily included brown regions are cuboid growth sectors, whereas these inclusion-free colorless regions are octahedral growth sectors.

In order to observe the distribution of inclusions and birefringence in mixed-habit diamonds, a polarizing microscope (Leica DM 4 P) was employed in this work. The microscope was equipped with a digital camera (Leica DMC 4500) and an image acquisition software (LAS V4.12).

The degree of plastic deformation and the strength of residual stress of diamonds were assessed by Raman spectra obtained by a Renishaw inVia Raman spectrometer fitted with a Leica DM 2500M microscope. Prior to mapping tests, the spectrometer was calibrated according to the 520.7 cm^{-1} peak of the silicon wafer (Kadlecikova et al., 2018). Raman mapping was conducted at room temperature using the laser with a wavelength of 532 nm, with grating of 2400 L mm^{-1} and aperture of 30×30 µm. All Raman spectra were collected under confocal mode with static scan ranging from 741.1 to

1880.5 cm^{-1}, with a laser power of 50 mW, an exposure time of 1s, and an accumulation of one. Collected spectra were fitted with a Lorentz function using WiRE 5.5 software to get more accurate values of the Raman shift and FWHM (full width at half maximum) of the diamond LO = TO bands.

The distribution of nitrogen and VN_3H defects (a kind of trigonal defect made up of a vacancy, a hydrogen atom, and three nitrogen atoms, Goss et al., 2014) in diamonds were determined by infrared spectra collected with a Nicolet iN10 MX spectrometer equipped with a MCT (mercury–cadmium–telluride) detector and a KBr beam splitter. The sample was placed on a KBr circular plate to collect transmission IR spectra in a 16-scan regime in the spectrum range of 675–6000 cm^{-1} with a spectrum resolution of 4 cm^{-1}. After the detector was cooled to liquid nitrogen temperature, mapping analysis was carried out at 50 µm intervals with an aperture of 50 × 50 µm. To cover the whole range of the sample, a total of 3710 absorption spectra were collected, and the baselines of all spectra were subtracted and normalized to convert absorbance to absorption coefficients of different peaks according to the intrinsic absorption of diamond. The real intensities of various nitrogen-related absorption peaks were calculated based on the formula proposed by Bokii et al. (1986), and the concentration of nitrogen was estimated using the ratios proposed by Boyd et al. (1994, 1995).

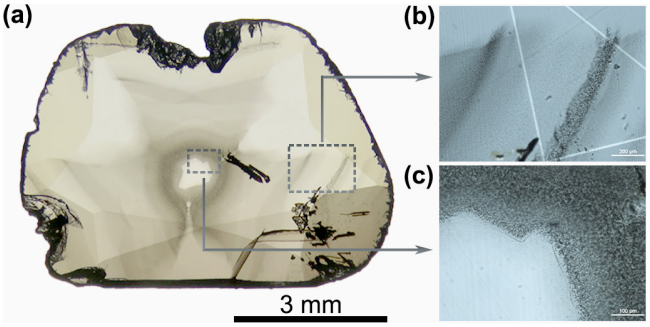

Figure 2. The distribution of graphite inclusions in Zimbabwean mixed-habit diamond (modified after Sun et al., 2022). **(a)** Color zoning of NDS-2 under mono-polarized light. **(b)** Parallel enriched bands of graphite inclusions in cuboid sectors. **(c)** Much smaller inclusions between octahedral sectors and cuboid sectors.

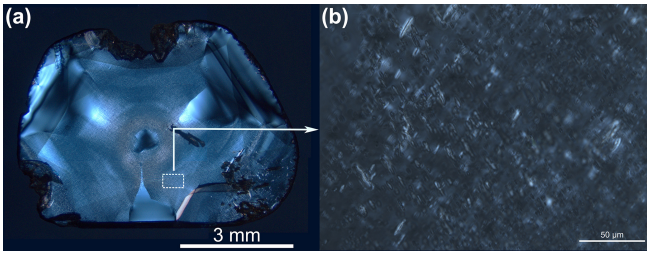

Figure 3. Birefringence in NDS-2 under cross-polarized light (modified after Sun et al., 2022). **(a)** Sharp straight birefringence patterns in octahedral sectors. **(b)** Birefringence caused by dense directional micro-cracks in cuboid sectors.

3 Results

3.1 Distribution of inclusions and birefringence

The mixed-habit diamond NDS-2 displayed apparent color sector zoning under mono-polarized light as a result of the differential distribution of inclusions (Fig. 2a): cuboid sectors were brown due to the existence of massive graphite inclusions, while octahedral sectors were colorless. In cuboid sectors, the graphite inclusions were distributed parallel to three (111) planes and intersected with each other at an angle of 120° (Sun et al., 2022). In addition, the distribution of graphite inclusions in cuboid regions was not totally uniform, and the relative enrichment of graphite inclusions would form parallel darker brown-colored bands, in which the density and grain size of graphite inclusions were both greater than those of lighter brown-colored areas (Fig. 2b). In NDS-2, graphite inclusions were the densest around the octahedral core, and a narrow band consisting of much smaller inclusions appeared as a transition band between the octahedral core and surrounding cuboid regions (Fig. 2c).

Under cross-polarized light, NDS-2 mainly showed two kinds of birefringence. One was the characteristic birefringence pattern only observed in mixed-habit diamonds that mimicked the shape of diamond growth band (Lang et al., 2007). This type of birefringence was more obvious in octahedral regions and was shown as black lobes that constantly twisted with the rotation of the sample. At certain positions, these black lobes would transform into sharp, straight birefringence patterns that were parallel to each other and consistently run through the entire octahedral region in a long distance. While in cuboid sectors, straight birefringence patterns were virtually undetectable owing to the influence of graphite inclusions (Fig. 3a). However, since graphite inclusions existed in directional micro-cracks of cuboid growth sectors, with the rotation of samples under cross-polarized light, black lobes that passed through the oval planes of the micro-cracks and twisted around the major axes of them would appear (Fig. 3b). These birefringence patterns would superimpose on each other to some extent and formed the overall birefringence of the whole diamond.

3.2 Strength of plastic deformation and residual stress

The occurrence of stress would change the lengths of bonds in crystal lattices, which thus affects vibration frequencies of bonds and is expected to result in shift of Raman bands compared to perfect strain-free crystals (Nasdala et al., 2005). Additionally, it has been determined that the FWHM of diamond Raman peak is highly sensitive to the disorder of diamond crystal (Stoneham, 1969); hence, it could be used to indicate the degree of plastic deformation (Erasmus et

al., 2011). Therefore, we could effectively analyze the strain characteristics of diamond crystals based on the Raman shift and FWHM of their LO + TO bands (Howell et al., 2010). The LO + TO band of unstressed diamond crystal is characterized for the peak position of 1332 cm^{-1} and the line width of 1.6 cm^{-1} (Grimsditch et al., 1978; Izraeli et al., 1999), while it would shift to higher wavenumbers with the increase in compressed stress and to lower wavenumbers with the increase in tensile stress (Nasdala et al., 2003).

Figure 4 shows an example of the Raman spectra of different growth sectors in NDS-2; it can be seen that the Raman shift of the octahedral growth sector was smaller than that of the cuboid growth sector, while the FWHM of LO + TO band of the octahedral growth sector was larger than that of the cuboid growth sector. And the differences were more pronounced in maps of Fig. 5. According to the map of the FWHM of LO + TO bands of NDS-2 (Fig. 5a), the FWHM of octahedral sectors, which was in the range of 3.8–4.5 cm^{-1}, was greater than that of cuboid sectors, which was about 3.2–3.7 cm^{-1}. This indicated that plastic deformation in octahedral sectors was stronger than that in cuboid sectors. Moreover, both sectors showed positive anomaly bands of the FWHM; however, these anomaly bands of the FWHM in octahedral sectors were relatively straight, while those in cuboid sectors were relatively curved. These anomaly bands could relate to one another to display the morphology and thickness of growth bands in different growth sectors of diamond. In addition, comparing Figs. 5a, Fig. 2a, and Fig. 3a, it can be seen that the positive anomaly bands of the FWHM in octahedral sectors could be correlated with straight birefringence patterns, and those in cuboid sectors could be correlated with the more enriched bands of graphite inclusions.

Figure 5b is the map of the Raman shift of the diamond LO + TO band; it was evident that the Raman shift of the whole sample was smaller than 1332 cm^{-1}, and there was a clear difference at the bottom of NDS-2, which should be accounted for by the uneven release of stress during cutting process. Despite these abnormal areas, the Raman shift of octahedral regions was about 1331.06–1331.12 cm^{-1}, and that of cuboid regions was about 1331.13–1331.18 cm^{-1}. This demonstrated that there was tensile residual stress in both growth regions, and larger shifts of the peak position in octahedral sectors meant that residual stress in these sectors was greater than that of cuboid sectors. Based on the equation between the residual stress and Raman shift of diamond proposed by Bergman and Nemanich (Bergman and Nemanich, 1995), it could be calculated that residual stress in octahedral sectors was about 0.46–0.49 GPa, and that in cuboid sectors was about 0.38–0.41 GPa. Moreover, negative anomaly bands of the Raman shift also showed up at growth bands where straight birefringence patterns and the relative enrichment of graphite inclusions appeared, and it was worth noting that these negative anomaly bands of the Raman shift corresponded to the positive anomalies of tensile residual stress in diamonds.

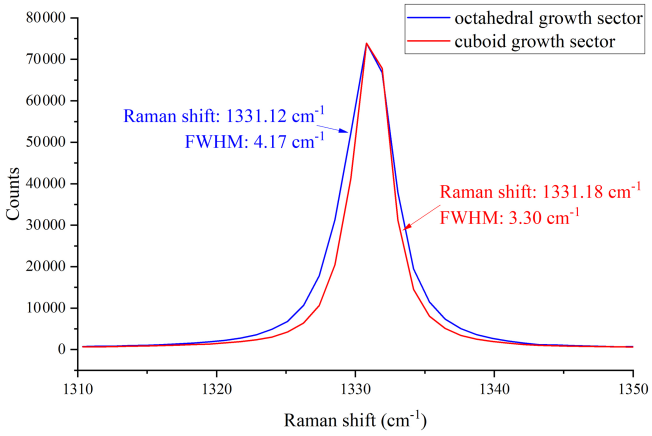

Figure 4. Two selected Raman spectra of different growth sectors in NDS-2; the blue line is the Raman band of the octahedral growth sector, and the red line is the Raman band of the cuboid growth sector.

3.3 Distribution of nitrogen and VN_3H defects

Nitrogen and hydrogen are two of the most common impurities in natural diamonds, both of which could exist in diamonds in various forms (Mainwood, 1994; Fritsch et al., 2007). However, due to the preferential incorporation of different impurities of different growth sectors, nitrogen-related defects are usually more enriched in octahedral sectors, while hydrogen-related IR-active defects are more enriched in cuboid sectors (Howell et al., 2012a). According to the FTIR absorption spectra in Fig. 6, we could see that nitrogen atoms in Zimbabwean mixed-habit diamonds mainly exist in the form of A centers (1282 cm^{-1}, a pair of neighboring substitutional nitrogen atoms, Davies, 1976), B centers (1010 cm^{-1}, four nitrogen atoms surrounding a vacancy, Woods, 1986), and a small amount of platelets (1382 cm^{-1}, consisting of carbon atoms and nitrogen atoms, Allen and Evans, 1981). Thus, these mixed-habit diamonds are attributed to type IaAB diamonds. Additionally, it was also clear that the absorption related to hydrogen (1405, 3050, 3107, 3236, 4496 cm^{-1}) in the cuboid sector was stronger than that of the octahedral sector.

The map of nitrogen concentration was shown in Fig. 7a. It was evident that the nitrogen concentrations of octahedral sectors were significantly higher than those of cuboid sectors, and in both growth sectors, nitrogen concentrations displayed an unstable decreasing trend from core to rim. In addition, the concentration of nitrogen presented obvious positive anomalies at growth bands showing straight birefringence patterns and the relative enrichment of graphite inclusions, and the nitrogen concentration of positive anomaly bands in octahedral sectors was also the highest of the whole sample.

The 3107 cm^{-1} peak, which is attributed to the absorption of VN_3H defects (Goss et al., 2014), is the most prominent hydrogen-related absorption peak in diamonds. According to

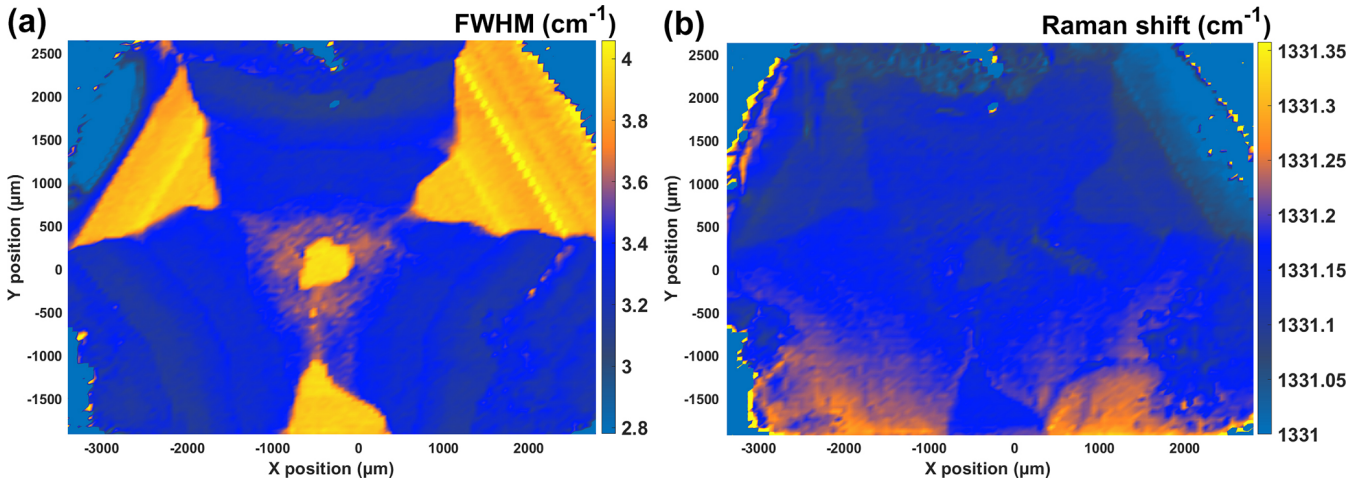

Figure 5. The maps of the **(a)** FWHM and **(b)** Raman shift of diamond LO = TO bands in NDS-2.

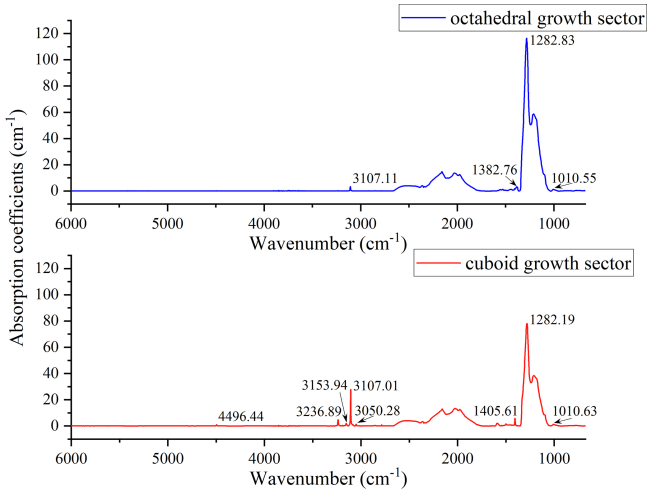

Figure 6. FTIR absorption spectra of different growth sectors in NDS-2.

the map of absorption coefficients of the 3107 cm^{-1} peak in Fig. 7b, the absorption coefficients of VN_3H defects in cuboid sectors were significantly higher than those in octahedral sectors, and the highest value of $\mu(3107)$ was around the octahedral core, which precisely corresponded to the densest area of graphite inclusions in cuboid sectors. In addition, the value of $\mu(3107)$ in cuboid sectors decreased steadily from core to rim, and it also showed positive anomalies in octahedral growth bands showing straight birefringence patterns and in cuboid growth bands enriched with graphite inclusions.

4 Discussion

Based on all the results above, straight birefringence patterns in octahedral sectors of Zimbabwean mixed-habit diamonds could be accurately connected with the enriched bands of graphite inclusions in cuboid sectors, and they all displayed positive anomalies of the FWHM and peak shift of Raman peaks (corresponding to stronger plastic deformation and larger residual stress), as well as the concentration of nitrogen and the absorption coefficients of VN_3H defects. Previous research suggested that the straight birefringence patterns that resembled the morphology of growth band were induced by the lattice parameter variation caused by the difference of nitrogen contents between different growth sectors (Howell, 2012). However, in this study, we hypothesized that the straight birefringence patterns in octahedral sectors and graphite enrichment bands in cuboid sectors might be induced by the same cause during the growth of diamonds based on the correlation between the distribution of straight birefringence patterns and graphite enrichment bands as well as the identical anomaly features they displayed.

Due to the fact that cuboid sectors grew faster than octahedral sectors over the majority of duration of crystallization (Rondeau et al., 2004), graphite inclusions were preferentially trapped in cuboid sectors of Zimbabwean mixed-habit diamonds (Smit et al., 2016). These graphite inclusions were mainly formed through graphitization of the host diamond and exist in dense directional micro-cracks in cuboid sectors of Zimbabwean mixed-habit diamonds (Sun et al., 2022). The occurrence of graphitization or the crystallization of graphite implied that the diamond had experienced annealing process of low pressure and high temperature, which usually happens above the temperature of 1150° in the mantle (Butenko et al., 2000), but it could also happen in the temperature range of 500–600° in the atmosphere containing oxygen or other oxidizers (Matsumoto et al., 1977). Moreover,

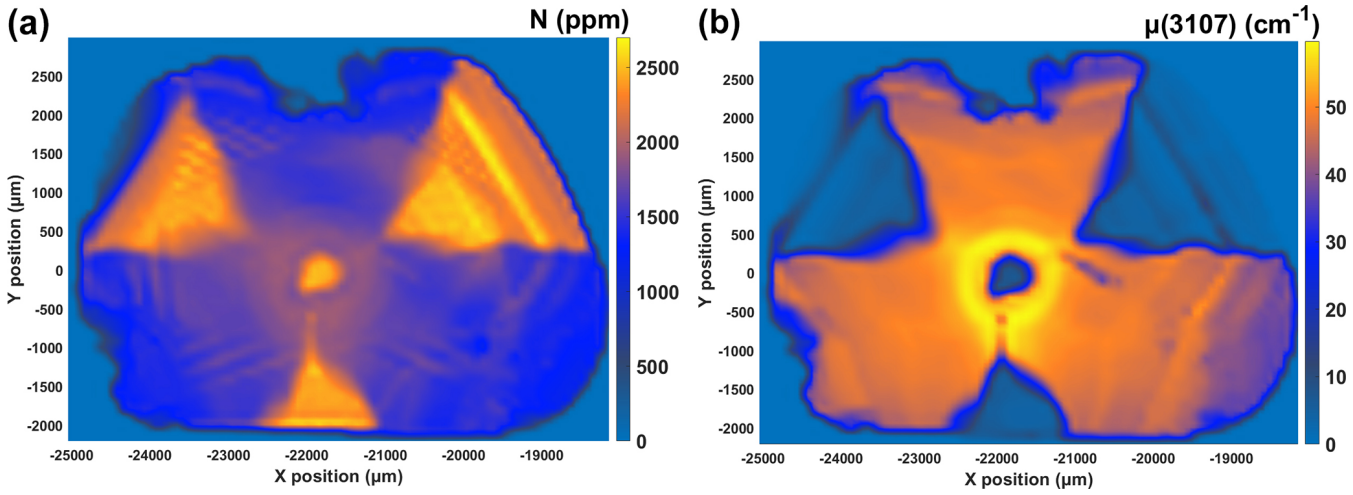

Figure 7. The maps of the **(a)** nitrogen concentration and **(b)** absorption coefficients of the 3107 cm^{-1} peak in NDS-2.

the relatively more enriched bands of graphite inclusions in certain growth bands of cuboid sectors in NDS-2 reflected that these growth bands had experienced more intense fluctuations of pressure and temperature during crystallization.

This assumption could also explain the straight birefringence patterns in octahedral sectors, the positive anomalies of residual stress, plastic deformation, nitrogen, and VN_3H defects in growth bands showing straight birefringence and the enrichment of graphite inclusions: under the conditions that were favorable to graphitization, metastable diamond would still crystallize (Nechaev and Khokhryakov, 2014), but its crystal lattice would be rather more disordered than that of diamond crystallized under diamond-stable conditions (Sokol et al., 2001). And because of the internal stress resulting from the lattice parameter variation between them, the shift of the peak position of the Raman band, which corresponded to the strength of residual stress, was greater at these more disordered growth bands (showing straight birefringence patterns and enrichment bands of graphite inclusions). And with the increase in tensile stress, the plastic deformation was further enhanced at these growth bands (Schroeder et al., 1995). As a result, birefringence that mimicked the morphology of these growth bands was formed in Zimbabwean mixed-habit diamonds.

In terms of the distribution of nitrogen and VN_3H defects in NDS-2, during crystallization of natural mixed-habit diamond in nitrogen, hydrogen-rich fluids and nitrogen and hydrogen atoms would first concentrate in octahedral sectors, but the nitrogen concentration limit is higher in octahedral sectors, while the hydrogen concentration limit is higher in cuboid sectors (Boyd et al., 1988; Burns et al., 1990); thus, the nitrogen contents of octahedral sectors were higher than those of cuboid sectors, and hydrogen-related defects were more enriched in cuboid sectors (Fig. 7). In addition, the nitrogen concentration limit of diamond could be impacted by the temperature of the external environment (Bursill and Glaisher, 1985); hence, when the temperature rose, the nitrogen concentration limit was elevated, and positive anomaly bands of nitrogen concentration were formed in Fig. 7a. Furthermore, under the same condition, diamond with more nitrogen atoms in its crystal lattice should also contain more VN_3H defects, because nitrogen atoms are the main constituents of VN_3H defects. This was also true in this investigation, as seen in Fig. 7a and b; the positive anomaly bands of nitrogen concentration and the positive anomaly bands of VN_3H defects appeared in identical growth bands.

5 Conclusions

In Zimbabwean mixed-habit diamonds, the growth bands showing straight birefringence patterns in octahedral sectors could be linked with growth bands enriched with graphite inclusions in cuboid sectors, and these growth bands were formed at same growth stages. Because of the comparatively intense fluctuations of temperature at these stages, nitrogen and VN_3H defects were more enriched in these growth bands of both sectors, while graphite inclusions were more enriched in cuboid growth bands. In addition, the lattices of diamond crystallized during these stages were more disordered, resulting in positive anomalies of residual stress and plastic deformation. This finding clearly demonstrated the correlation between birefringence and spectroscopic properties of diamonds, which furthered the understanding of the formation of birefringence as well as the relationship between impurities, strain, and birefringence in natural diamonds.

Data availability. Data sets used in this paper are available upon proper request.

Author contributions. CS conducted all experiments and wrote the paper, TL provided all samples used in this study and hosted one program leading to this publication, MH analyzed results related to Raman mapping, ZS helped improve the expressions of this paper, and YD analyzed the distribution of nitrogen in samples.

Competing interests. The contact author has declared that none of the authors has any competing interests.

Disclaimer. Publisher's note: Copernicus Publications remains neutral with regard to jurisdictional claims in published maps and institutional affiliations.

Acknowledgements. The authors appreciate the valuable comments of the two anonymous referees that helped improve this paper and thank Ye Yuan from the lab of the School of Gemology, China University of Geosciences (Beijing), for his valuable advice and support.

Financial support. This research has been supported by the National Infrastructure of Mineral, Rock and Fossil Resources (grant no. K1603901); the National Science Foundation of China (grant no. 42073008); and the scientific research program of National Gems & Jewelry Testing Co. Ltd. (grant no. NGTC20210700).

Review statement. This paper was edited by Paola Comodi and reviewed by two anonymous referees.

References

Agrosì, G., Tempesta, G., Scandale, E., and Harris, J. W.: Growth and post-growth defects in a diamond from Finsch mine (South Africa), Eur. J. Mineral., 25, 551–559, https://doi.org/10.1127/0935-1221/2013/0025-2301, 2013.

Agrosì, G., Tempesta, G., Della Ventura, G., Cestelli Guidi, M., Hutchison, M., Nimis, P., and Nestola, F.: Non-Destructive In Situ Study of Plastic Deformations in Diamonds: X-ray Diffraction Topography and μFTIR Mapping of Two Super Deep Diamond Crystals from São Luiz (Juina, Brazil), Crystals, 7, 233, https://doi.org/10.3390/cryst7080233, 2017.

Allen, B. P. and Evans, T.: Aggregation of Nitrogen in Diamond, Including Platelet Formation, Proc. R. Soc. Lond. A, 375, 93–104, https://doi.org/10.1098/rspa.1981.0041, 1981.

Balzaretti, N. M. and daJornada, J. A. H.: Pressure dependence of the refractive index of diamond, cubic silicon carbide and cubic boron nitride, Solid State Commun., 99, 943–948, https://doi.org/10.1016/0038-1098(96)00341-9, 1996.

Bergman, L. and Nemanich, R. J.: Raman and Photoluminescence Analysis of Stress State and Impurity Distribution in Diamond Thin-Films, J. Appl. Phys., 78, 6709–6719, https://doi.org/10.1063/1.360495, 1995.

Bokii, G. B., Bezrukov, G.N., Kluev, J. A., Naletov, A. M., and Nepsha, V. I.: Natural and synthetic diamonds, Nauka, Moscow, Russia, 1986 (in Russian).

Boyd, S. R., Pillinger, C. T., Milledge, H. J., Mendelssohn, M. J., and Seal, M.: Fractionation of Nitrogen Isotopes in a Synthetic Diamond of Mixed-Crystal Habit, Nature, 331, 604–607, https://doi.org/10.1038/331604a0, 1988.

Boyd, S. R., Kiflawi, I., and Woods, G. S.: The Relationship between Infrared-Absorption and the a Defect Concentration in Diamond, Philos. Mag. B, 69, 1149–1153, https://doi.org/10.1080/01418639408240185, 1994.

Boyd, S. R., Kiflawi, I., and Woods, G. S.: Infrared-Absorption by the B-Nitrogen Aggregate in Diamond, Philos. Mag. B, 72, 351–361, https://doi.org/10.1080/13642819508239089, 1995.

Bureau, H., Frost, D. J., Bolfan-Casanova, N., Leroy, C., Esteve, I., and Cordier, P.: Diamond growth in mantle fluids, Lithos, 265, 4–15, https://doi.org/10.1016/j.lithos.2016.10.004, 2016.

Burns, R. C., Cvetkovic, V., Dodge, C. N., Evans, D. J. F., Rooney, M. L. T., Spear, P. M., and Welbourn, C. M.: Growth-Sector Dependence of Optical-Features in Large Synthetic Diamonds, J. Cryst. Growth, 104, 257–279, https://doi.org/10.1016/0022-0248(90)90126-6, 1990.

Bursill, L. A. and Glaisher, R. W.: Aggregation and Dissolution of Small and Extended Defect Structures in Type-Ia Diamond, Am. Mineral., 70, 608–618, 1985.

Butenko, Y. V., Kuznetsov, V. L., Chuvilin, A. L., Kolomiichuk, V. N., Stankus, S. V., Khairulin, R. A., and Segall, B.: Kinetics of the graphitization of dispersed diamonds at "low" temperatures, J. Appl. Phys., 88, 4380–4388, https://doi.org/10.1063/1.1289791, 2000.

Chen, N., Zhang, G., Li, R., Xu, G., Wang, F., Ma, H., and Jia, X.: Defect and Stress Reduction in High-Pressure and High-Temperature Synthetic Diamonds Using Gradient Cooling Technology, Cryst. Growth Des., 20, 3358–3364, https://doi.org/10.1021/acs.cgd.0c00148, 2020.

Connell, S. H., Sellschop, J. P. F., Butler, J. E., Maclear, R. D., Doyle, B. P., and Machi, I. Z.: A study of the mobility and trapping of minor hydrogen concentrations in diamond in three dimensions using quantitative ERDA microscopy, Diamond Relat. Mater., 7, 1714–1718, https://doi.org/10.1016/S0925-9635(98)00266-0, 1998.

Davies, G.: The A nitrogen aggregate in diamond-its symmetry and possible structure, J. Phys. C:, 9, L537, https://doi.org/10.1088/0022-3719/9/19/005, 1976.

Eaton-Magaña, S., Ardon, T., and Zaitsev, A. M.: Inclusion and point defect characteristics of Marange graphite-bearing diamonds after high temperature annealing, Diamond Relat. Mater., 71, 20–29, https://doi.org/10.1016/j.diamond.2016.11.011, 2017.

Erasmus, R. M., Daniel, R. D., and Comins, J. D.: Three-dimensional mapping of stresses in plastically deformed diamond using micro-Raman and photoluminescence spectroscopy, J. Appl. Phys., 109, 013527, https://doi.org/10.1063/1.3531548, 2011.

Fritsch, E., Hainschwang, T., Massi, L., and Rondeau, B.: Hydrogen-related optical centers in natural diamond: An update, New Diam. Front. C Tec., 17, 63–89, 2007.

Glazer, A. M., Lewis, J. G., and Kaminsky, W.: An automatic optical imaging system for birefringent media, P. Roy. Soc. A, 452, 2751–2765, https://doi.org/10.1098/rspa.1996.0145, 1996.

Goss, J. P., Briddon, P. R., Hill, V., Jones, R., and Rayson, M. J.: Identification of the structure of the 3107 cm^{-1} H-related defect in diamond, J. Phys. Condens. Matter., 26, 145801, https://doi.org/10.1088/0953-8984/26/14/145801, 2014.

Grimsditch, M. H., Anastassakis, E., and Cardona, M.: Effect of uniaxial stress on the zone-center optical phonon of diamond, Phys. Rev. B, 18, 901–904, https://doi.org/10.1103/PhysRevB.18.901, 1978.

Grimsditch, M. H., Anastassakis, E., and Cardona, M.: Piezobirefringence in diamond, Phys. Rev. B, 19, 3240–3243, https://doi.org/10.1103/PhysRevB.19.3240, 1979.

Howell, D.: Strain-induced birefringence in natural diamond: a review, Eur. J. Mineral., 24, 575–585, https://doi.org/10.1127/0935-1221/2012/0024-2205, 2012.

Howell, D., Wood, I. G., Dobson, D. P., Jones, A. P., Nasdala, L., and Harris, J. W.: Quantifying strain birefringence halos around inclusions in diamond, Contrib. Mineral. Petr., 160, 705–717, https://doi.org/10.1007/s00410-010-0503-5, 2010.

Howell, D., O'Neill, C. J., Grant, K. J., Griffin, W. L., Pearson, N. J., and O'Reilly, S. Y.: μ-FTIR mapping: Distribution of impurities in different types of diamond growth, Diamond Relat. Mater., 29, 29–36, https://doi.org/10.1016/j.diamond.2012.06.003, 2012a.

Howell, D., O'Neill, C. J., Grant, K. J., Griffin, W. L., O'Reilly, S. Y., Pearson, N. J., Stern, R. A., and Stachel, T.: Platelet development in cuboid diamonds: insights from micro-FTIR mapping, Contrib. Mineral. Petr., 164, 1011–1025, https://doi.org/10.1007/s00410-012-0786-9, 2012b.

Howell, D., Griffin, W. L., Piazolo, S., Say, J. M., Stern, R. A., Stachel, T., Nasdala, L., Rabeau, J. R., Pearson, N. J., and O'Reilly, S. Y.: A spectroscopic and carbon-isotope study of mixed-habit diamonds: Impurity characteristics and growth environment, Am. Mineral., 98, 66–77, https://doi.org/10.2138/am.2013.4179, 2013.

Izraeli, E. S., Harris, J. W., and Navon, O.: Raman barometry of diamond formation, Earth Planet. Sc. Lett., 173, 351–360, https://doi.org/10.1016/S0012-821x(99)00235-6, 1999.

Kadlecikova, M., Breza, J., Vanco, L., Mikolasek, M., Hubenak, M., Racko, J., and Gregus, J.: Raman spectroscopy of porous silicon substrates, Optik, 174, 347–353, https://doi.org/10.1016/j.ijleo.2018.08.084, 2018.

Kanda, H. and Watanabe, K.: Distribution of the cobalt-related luminescence center in HPHT diamond, Diamond Relat. Mater., 6, 708–711, https://doi.org/10.1016/S0925-9635(96)00666-8, 1997.

Kurtz, A. D., Kulin, S. A., and Averbach, B. L.: Effect of Dislocations on the Minority Carrier Lifetime in Semiconductors, Phys. Rev., 101, 1285–1291, https://doi.org/10.1103/PhysRev.101.1285, 1956.

Lang, A. R.: Causes of Birefringence in Diamond, Nature, 213, 248–251, https://doi.org/10.1038/213248a0, 1967.

Lang, A. R., Yelisseyev, A. P., Pokhilenko, N. P., Steeds, J. W., and Wotherspoon, A.: Is dispersed nickel in natural diamonds associated with cuboid growth sectors in diamonds that exhibit a history of mixed-habit growth?, J. Cryst. Growth, 263, 575–589, https://doi.org/10.1016/j.jcrysgro.2003.11.116, 2004.

Lang, A. R., Bulanova, G. P., Fisher, D., Furkert, S., and Sarua, A.: Defects in a mixed-habit Yakutian diamond: Studies by optical and cathodoluminescence microscopy, infrared absorption, Raman scattering and photoluminescence spectroscopy, J. Cryst. Growth, 309, 170–180, https://doi.org/10.1016/j.jcrysgro.2007.09.022, 2007.

Mainwood, A.: Nitrogen and Nitrogen-Vacancy Complexes and Their Formation in Diamond, Phys. Rev. B, 49, 7934–7940, https://doi.org/10.1103/PhysRevB.49.7934, 1994.

Masuya, S., Hanada, K., Oshima, T., Sumiya, H., and Kasu, M.: Formation of stacking fault and dislocation behavior during the high-temperature annealing of single-crystal HPHT diamond, Diamond Relat. Mater., 75, 155–160, https://doi.org/10.1016/j.diamond.2017.04.003, 2017.

Matsumoto, S., Kanda, H., Sato, Y., and Setaka, N.: Thermal desorption spectra of the oxidized surfaces of diamond powders, Carbon, 15, 299–302, https://doi.org/10.1016/0008-6223(77)90034-3, 1977.

Nasdala, L., Brenker, F. E., Glinnemann, J., Hofmeister, W., Gasparik, T., Harris, J. W., Stachel, T., and Reese, I.: Spectroscopic 2D-tomography: Residual pressure and strain around mineral inclusions in diamonds, Eur. J. Mineral., 15, 931–935, https://doi.org/10.1127/0935-1221/2003/0015-0931, 2003.

Nasdala, L., Hofmeister, W., Harris, J. W., and Glinnemann, J.: Growth zoning and strain patterns inside diamond crystals as revealed by Raman maps, Am. Mineral., 90, 745–748, https://doi.org/10.2138/am.2005.1690, 2005.

Nasdala, L., Grambole, D., Wildner, M., Gigler, A. M., Hainschwang, T., Zaitsev, A. M., Harris, J. W., Milledge, J., Schulze, D. J., Hofmeister, W., and Balmer, W. A.: Radio-colouration of diamond: a spectroscopic study, Contrib. Mineral. Petr., 165, 843–861, https://doi.org/10.1007/s00410-012-0838-1, 2013.

Nechaev, D. V. and Khokhryakov, A. F.: Formation of metastable graphite inclusions during diamond crystallization in model systems, Geol. Ore. Deposit+, 56, 139–146, https://doi.org/10.1134/S1075701514020044, 2014.

Rondeau, B., Fritsch, E., Guiraud, M., Chalain, J. P., and Notari, F.: Three historical "asteriated" hydrogen-rich diamonds: growth history and sector-dependent impurity incorporation, Diamond Relat. Mater., 13, 1658–1673, https://doi.org/10.1016/j.diamond.2004.02.002, 2004.

Schroeder, S., Frankel, J., and Abbate, A.: The Relationship between Residual Stress and Hardness and the Onset of Plastic Deformation, Army Armament Research Development and Engineering Center Watervliet Ny Benet Labs, https://doi.org/10.21236/ada302173, 1995.

Sellschop, J. P. F. and Field, J. E. (Eds.): Nuclear probes in the study of diamond, Properties of natural and synthetic diamond, Academic Press, London, England, ISBN 0-12-255352-7, 1992.

Skuzovatov, S. Y., Zedgenizov, D. A., Shatsky, V. S., Ragozin, A. L., and Kuper, K. E.: Composition of cloudy microinclusions in cctahedral diamonds from the Internatsional'naya kimberlite pipe (Yakutia), Russian Geol. Geophys., 52, 85–96, https://doi.org/10.1016/j.rgg.2010.12.007, 2011.

Smit, K. V., Shirey, S. B., Stern, R. A., Steele, A., and Wang, W.: Diamond growth from C–H–N–O recycled fluids in the lithosphere: Evidence from CH_4 micro-inclusions and $\delta^{13}C$–$\delta^{15}N$–N content in Marange mixed-habit diamonds, Lithos, 265, 68–81, https://doi.org/10.1016/j.lithos.2016.03.015, 2016.

Smit, K. V., Myagkaya, E., Persaud, S., and Wang, W. Y.: Black Diamonds from Marange (Zimbabwe): A Result of Natural Irradiation and Graphite Inclusions, Gems. Gemol., 54, 132–148, https://doi.org/10.5741/Gems.54.2.132, 2018.

Smith, E. M. and Wang, W.: Fluid CH_4 and H_2 trapped around metallic inclusions in HPHT synthetic diamond, Diamond Relat. Mater., 68, 10–12, https://doi.org/10.1016/j.diamond.2016.05.010, 2016.

Sokol, A. G., Pal'yanov, Y. N., Pal'yanova, G. A., Khokhryakov, A. F., and Borzdov, Y. M.: Diamond and graphite crystallization from C-O-H fluids under high pressure and high temperature conditions, Diamond Relat. Mater., 10, 2131–2136, https://doi.org/10.1016/S0925-9635(01)00491-5, 2001.

Stoneham, A. M.: Shapes of Inhomogeneously Broadened Resonance Lines in Solids, Rev. Modern Phys., 41, 82–108, https://doi.org/10.1103/RevModPhys.41.82, 1969.

Sun, C. Y., Lu, T. J., Song, Z. H., He, M. Y., and Deng, Y.: Analysis of Abnormal Birefringence and Graphite Inclusions in Zimbabwean Diamonds, Rock Miner. Anal., 41, 199–210, https://doi.org/10.15898/j.cnki.11-2131/td.202111050165, 2022.

Weiss, Y., Kessel, R., Griffin, W. L., Kiflawi, I., Klein-BenDavid, O., Bell, D. R., Harris, J. W., and Navon, O.: A New model for the evolution of diamond-forming fluids: evidence from Mmicroinclusion-bearing diamonds from Kankan, Guinea, Lithos, 112, 660–674, https://doi.org/10.1016/j.lithos.2009.05.038, 2009.

Woods, G. S.: Platelets and the Infrared-Absorption of Type-Ia Diamonds, Proc. R. Soc. Lond. A, 407, 219–238, https://doi.org/10.1098/rspa.1986.0094, 1986.

Zedgenizov, D. A., Kagi, H., Shatsky, V. S., and Sobolev, N. V.: Carbonatitic melts in cuboid diamonds from Udachnaya kimberlite pipe (Yakutia): evidence from vibrational spectroscopy, Mineral. Mag., 68, 61–73, https://doi.org/10.1180/0026461046810171, 2004.